PERGAMON

Deep-Sea Research I 49 (2002) 1–17

DEEP-SEA RESEARCH
PART I

www.elsevier.com/locate/dsr

Seasonal and interannual modulation of mixed layer variability at 0°, 110°W

Meghan F. Cronin*, William S. Kessler

National Oceanographic and Atmospheric Administration (NOAA), Pacific Marine Environmental Laboratory (PMEL), 7600 Sand Point Way NE, Seattle, WA 98115, USA

Received 22 August 2000; received in revised form 9 April 2001; accepted 29 June 2001

Abstract

Long, high resolution time series from the 0°, 110°W tropical atmosphere ocean mooring in the eastern equatorial Pacific are used to analyze how warm and cold phases of El Niño-Southern Oscillation (ENSO) and the annual cycle modulate the near-surface stratification and sea-surface temperature (SST) diurnal cycle. During the annual warm season (February–April), when solar warming is large and wind mixing weak, the isothermal-mixed layer depth (MLD_T) is shallow (typically 10 m deep) and the 1 m SST diurnal cycle amplitude is large (typically up to 0.4°C). Likewise during the remainder of the year when SST is generally cool, typically the diurnal cycle amplitude is less than 0.2°C and the isothermal-mixed layer is deeper than 20 m. Thus, annual variations in wind and insolation, which lead to an annual cycle in SST, also cause annual modulation of the SST diurnal cycle and near-surface stratification, consistent with one-dimensional mixed layer physics. However, on interannual time scales, mixed layer physics are more complicated. In particular, the diurnal cycle amplitude and MLD_T anomalies are out of phase with the SST anomalies. MLD_T is anomalously deep and the SST diurnal cycle amplitude is anomalously low during the warm phase of ENSO. On these longer timescales, MLD_T tends to be strongly influenced by thermocline-depth variability. In addition, salinity stratified barrier layers large enough to support temperature inversions were often observed at 0°, 110°W during the final stage of El Niños. As SST rose above 28.5°C during the final stage of the 1997–1998 El Niño, a regime shift was observed, with large temperature inversions, a relative increase in SST diurnal cycle amplitude, and large variability in the mixed-layer depth. It is likely that barrier layers (inferred from temperature inversions) allowed warm conditions to remain, even as the thermocline and mixed-layer depths shoaled.

Keywords: Diurnal variations; Diurnal thermocline; Surface mixed layer; Seasonal variations; El Niño; Temperature inversions

1. Introduction

Sea-surface temperature variability in the eastern equatorial Pacific occurs primarily within four frequency bands (Kessler et al., 1996): a diurnal cycle associated with daytime warming and nighttime cooling; a 20–40 day band associated with tropical instability waves; an annual cycle, which is dominant despite the fact that the sun crosses the equator twice per year; and a 2–7 year band associated with the El Niño/Southern Oscillation (ENSO) cycle. There has been considerable work showing the cross-scale interactions at the lower end of the spectrum, such as phase locking between ENSO and the annual cycle (Rasmusson

*Corresponding author. Fax: +1-206-526-6744.
E-mail address: cronin@pmel.noaa.gov (M.F. Cronin).

0967-0637/01/$ - see front matter
PII: S0967-0637(01)00043-7

and Carpenter, 1982; Deser and Wallace, 1987; Xie, 1995; Harrison and Larkin, 1998) and annual and interannual modulation of tropical instability waves (Halpern et al., 1988; Qiao and Weisberg, 1995, 1998). In this paper we investigate the cross-scale interaction with the high end of the spectrum. In particular, we investigate how the warm and cold phases of ENSO and the seasonal cycle modulate and in turn are affected by the diurnal cycle in SST and short lived temperature inversions.

Solar warming occurs only during the daytime, and mixing occurs primarily at nighttime in regions of light winds (Moum et al., 1989; Peters et al., 1994; Bond and McPhaden, 1995). Thus, seasonal and interannual variations in wind mixing and surface heating can be expected to cause variations in the SST diurnal cycle, as well as seasonal and interannual variations in SST. For example, increased wind mixing will tend to both cool the SST and reduce the SST diurnal cycle, and solar warming will tend to both warm the SST and increase the SST diurnal cycle. Thus, based on simple one-dimensional mixed layer physics, one might expect an increased SST diurnal cycle during warm phases of the low-frequency SST variability. Further, since increased solar warming and reduced wind mixing (which give rise to a large SST diurnal cycle) also tend to cause surface thermal restratification, one might also expect a shallow isothermal-mixed layer, separated from the deeper thermocline by a fossil layer, during the warm phases.

However, in general, eastern equatorial Pacific SST is controlled by complicated physics that are not purely one-dimensional. For example, at the equator, the thermocline can respond both to Kelvin waves generated by remote wind-forcing and to Ekman upwelling and downwelling caused by local variations in zonal wind. On seasonal time scales, the equatorial trade winds vary in relation to the meridional location of the intertropical convergence zone (ITCZ) (Fig. 1). In Figs. 1–3 low outgoing longwave radiation (OLR) indicates the presence of cold cloud tops (e.g. tall cumulus towers) associated with deep tropical convection. Low-level, hence relatively warm, stratus clouds that often form over seasonally cool SST are indistinguishable from the surface in the OLR records. Weak winds and deep convection associated with the ITCZ are far north of the equator during the cold season (August–October), when the equatorial cold tongue is fully formed, and are nearest to the equator during the warm season (February–April), when the equatorial waters are warmest (Fig. 1). On interannual time scales, equatorial trade winds vary in relation to the zonal location of the warm pool's deep atmospheric convection (Figs. 2 and 3). During El Niño events, the warm pool, deep convection and trade winds feeding into the convection, all shift eastward. During La Niña events, the system shifts westward. On both seasonal and interannual time scales, the tropical Pacific ocean and atmosphere are coupled, so that variations in insolation and trade wind forcing are both caused by variations in the SST pattern and also generate changes in the SST through surface-heat fluxes, mixing, and horizontal and vertical advection.

Adding to the complicated dynamics in the eastern equatorial Pacific, since the thermocline is very shallow in this region, mixing and vertical advection can bring very cool water to the surface (Figs. 2 and 3). Indeed, because the mean thermocline is so shallow, thermocline variability is often used as a proxy for mixed layer depth variability in the eastern equatorial Pacific (Xie, 1995). Thus, we pose the following questions: (1) If the SST diurnal cycle is affected primarily by surface one-dimensional mixed layer processes (e.g. wind mixing, solar warming), processes that also affect the lower frequency SST variability, what is the relationship between the SST diurnal cycle and lower frequency SST anomalies? Is the SST diurnal cycle larger during the warm phases? (2) Since the thermocline is so shallow in the eastern tropical Pacific, is it reasonable to use thermocline-depth variability as a proxy for mixed-layer depth variability?

2. Data

Data used in this analysis are primarily from the 0°, 110°W tropical atmosphere ocean (TAO) mooring. Originally supported by NOAA's Equa-

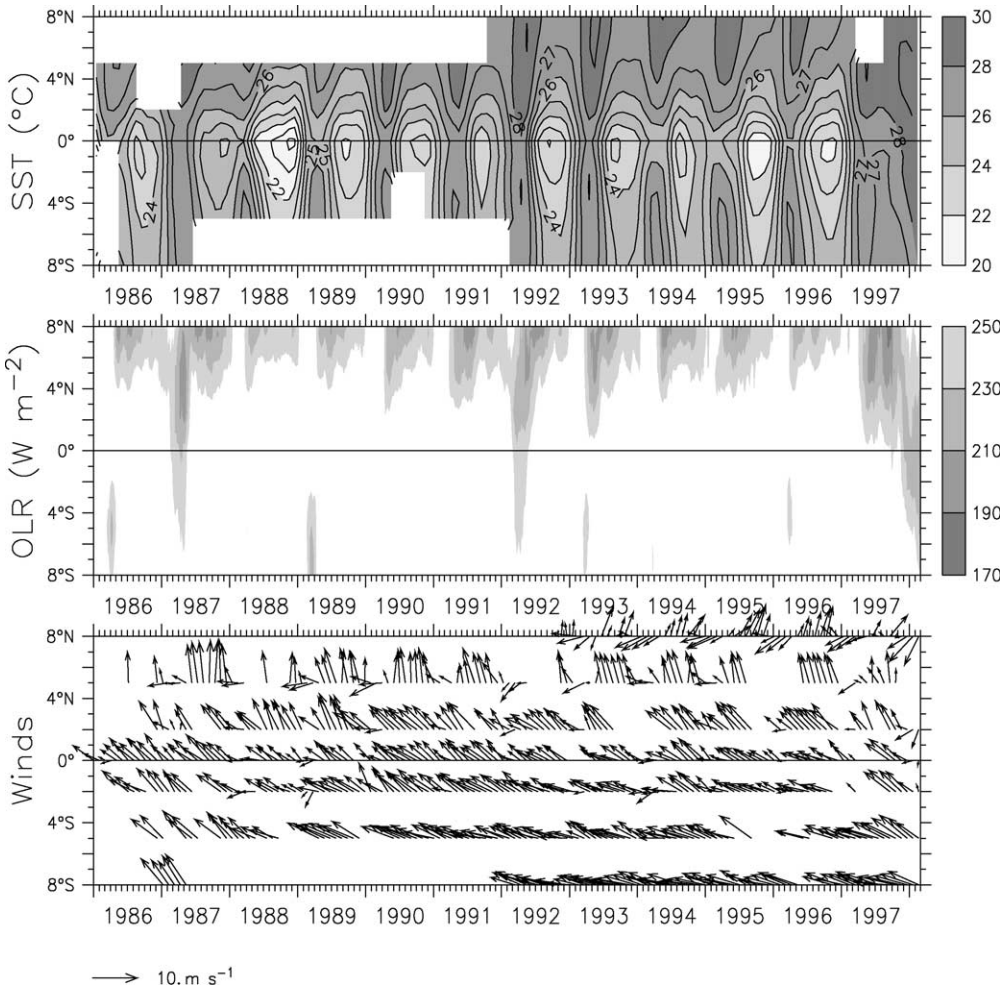

Fig. 1. Time-latitude plot of 110°W monthly averaged sea-surface temperature (SST), outgoing longwave radiation (OLR), and wind vectors from January 1986 through February 1998.

torial Pacific Ocean Climate Studies (EPOCS) program (Halpern, 1987) and later incorporated into the TAO array (McPhaden et al., 1998), the mooring has one of the longest time series of the array, extending back to 1980. With approximately 70 moorings in the tropical Pacific, the TAO array was designed to improve monitoring, understanding, and forecasting of ENSO. Standard measurements on all TAO moorings include hourly surface wind speed and direction, air temperature, relative humidity, 1 m depth SST, and daily averaged subsurface temperatures. At several of the sites, including 0°, 110°W, ocean temperature was measured by miniature temperature recorders (MTRs) with a sample rate of typically 10–20 min. MTR depths were typically 1, 10, 25, 45, 60, 80, 100, 120, 140, 200, 300, and 500 m. At other eastern Pacific TAO moorings, vertical resolution of temperature was typically 20 m above 140 m, not sufficient to resolve mixed-layer depth.

During the August 1997 deployment, the mooring was also enhanced with an optical rain gauge (ORG), a Seabird Electronics conductivity and

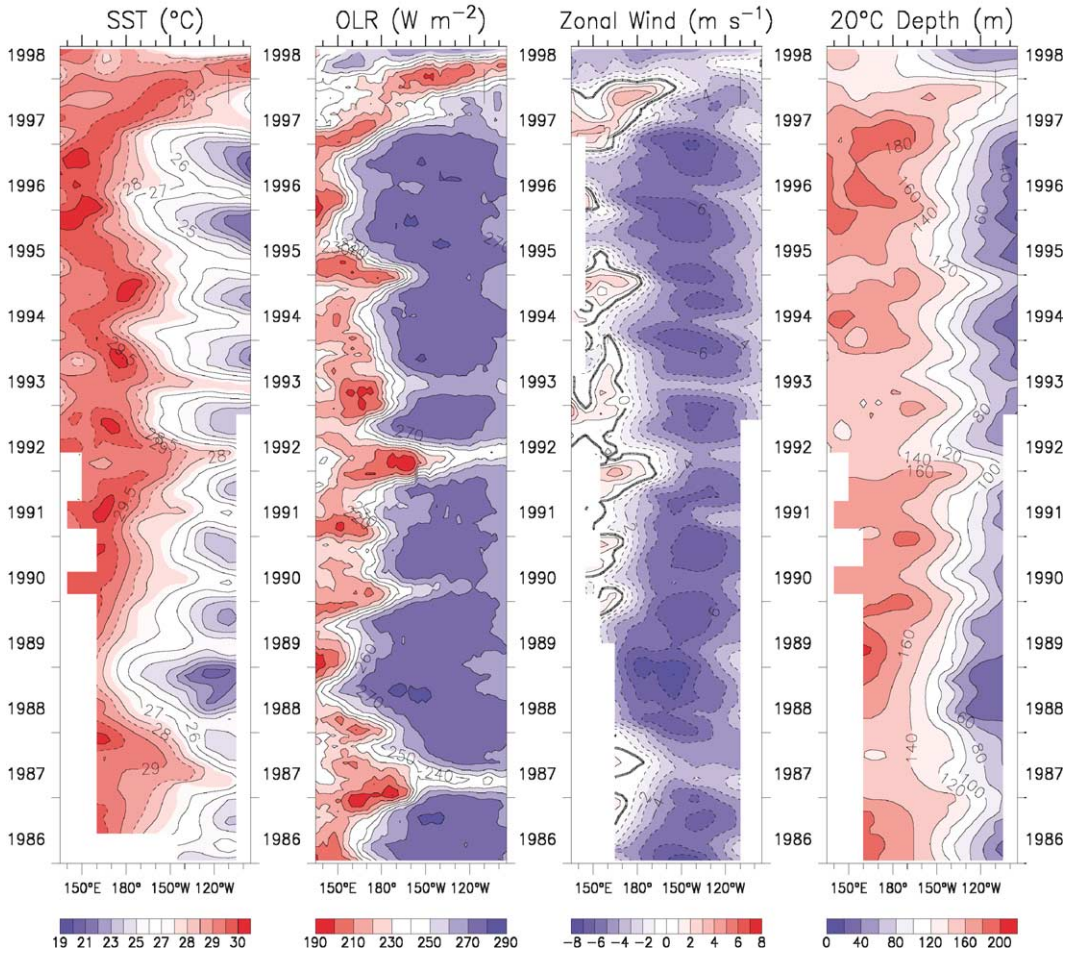

Fig. 2. Time-longitude plot of equatorial SST, OLR, zonal winds, and depth of the 20°C isotherm (Z20) from June 1986 through June 1998. Zonal wind, Z20 and SST are measured by TAO buoys. At each longitude, monthly means from buoys at 2°S, 0°, 2°N are averaged to produce the equatorial value then filtered in time with a 1-2-1 filter. The black line along 110°W longitude from September 1997 through February 1998 indicates the time and location of the high resolution monitoring.

temperature sensor at 1 m to monitor sea surface salinity[1] (SSS), and a set of additional MTRs so that hourly averaged subsurface temperature had 5 m vertical resolution within the top 50 m. The period from August 1997 through February 1998 spans the peak stage of the historic 1997–1998 El Niño and will be referred to as the enhanced monitoring period (EMP).

For all TAO moorings, daily averaged surface data (including SST) are telemetered via satellite in near real-time; hourly surface data and all MTR subsurface temperature data are available only after recovery of the mooring. Thus, mooring failure and vandalism can cause data gaps for up to full deployment periods in the hourly and subsurface MTR data, and for generally shorter periods in the daily averaged telemetered data. Because of an extensive gap after February 1998 in the subsurface data, our analysis will extend only until February 1998, the end of the EMP. Hourly

[1] Salinity is reported on the PSS-78 scale (Lewis and Fofonoff, 1979), which is denoted in this paper by PSU (practical salinity unit).

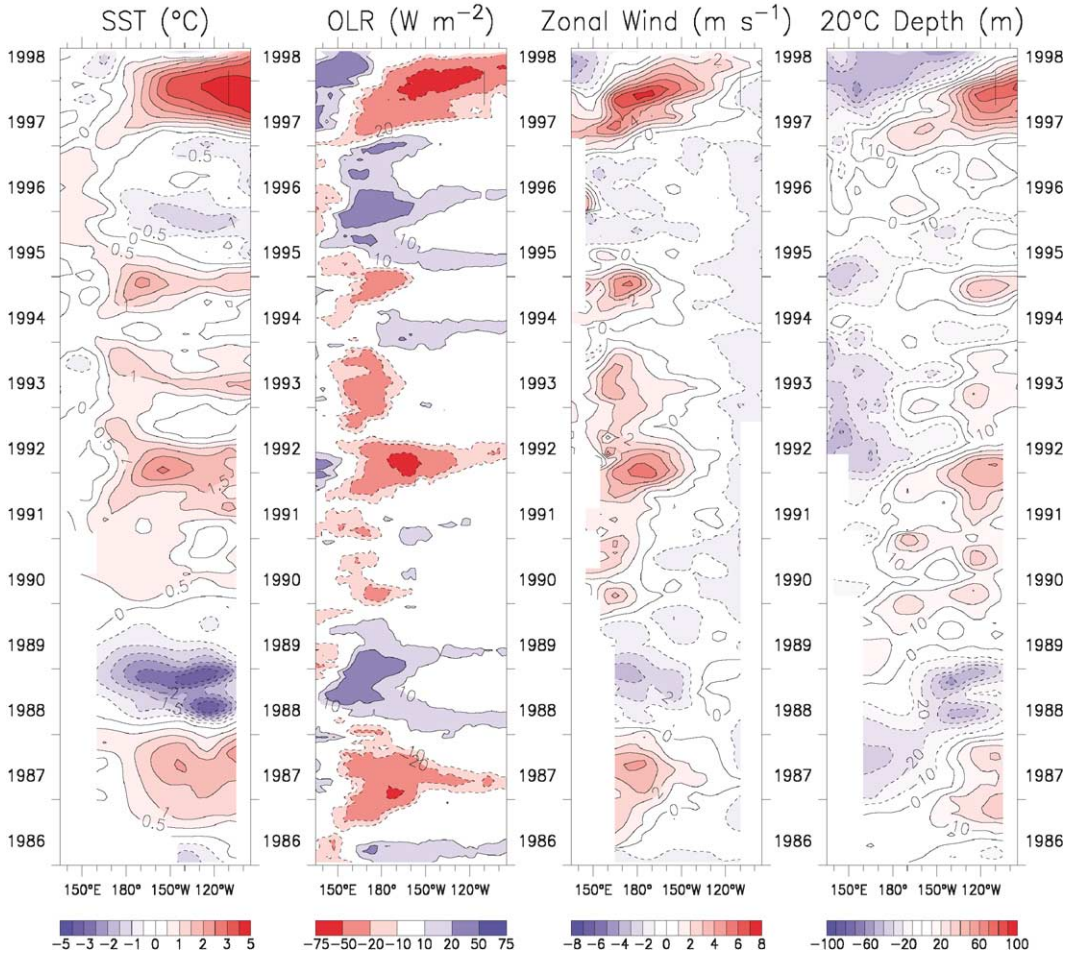

Fig. 3. Time-longitude plot of interannual anomalous equatorial band SST, OLR, zonal winds, and Z20 from June 1986 through June 1998. The anomalies are computed by subtracting the 1984–1998 seasonal climatologies from the fields shown in Fig. 2. As in Fig. 2, the black line indicates high-resolution monitoring.

data at 0°, 110°W began in late 1985 and encompasses at least part of five El Niños (1986–1987, 1991–1992, 1993, 1994–1995, and 1997–1998), and two La Niñas (1988 and 1996). Daily averaged data have more complete records and also include the 1982–1983 El Niño.

In our analysis, we define the near-isothermal-mixed layer depth (hereinafter referred to as MLD_T) as the depth at which the subsurface temperature is 0.5°C cooler than the SST, i.e.

$$MLD_T = z(T = \mathrm{SST} - 0.5^{\circ}\mathrm{C}). \quad (1)$$

MLD_T is distinct from the near-isopycnal "mixed-layer depth" (MLD), which is defined in terms of density. In regions with a near-surface freshwater stratification, the mixed-layer depth MLD can be shallower than the isothermal-mixed layer depth MLD_T. The layer between the shallow MLD and deeper MLD_T is often referred to as a "barrier layer" since the salinity gradient isolates the surface from the cool thermocline water and acts as a barrier to turbulent mixing of heat (Lukas and Lindstrom, 1991). However, without subsurface salinity data, MLD cannot be directly evaluated and barrier layers can only be inferred from temperature inversions, which must

be supported by a salinity stratification to remain stable.

Analyses of the upper ocean (near isothermal) temperature stratification require very accurate temperature measurements with high vertical resolution. Errors in MLD_T due to vertical resolution are estimated as a fraction m of the depth difference (Δz) between the spanning sensors:

$$er(MLD_T) = m\Delta z. \quad (2)$$

For linear stratification, m will be near zero; but for step-like stratification, m can approach one. Since the stratification is unknown between temperature sensors, we use a value of 0.5 for m. Thus, a 5 m vertical resolution (as for example during the EMP) corresponds to a MLD_T error of 2.5 m. On the basis of laboratory predeployment and postdeployment calibrations, MTR temperature accuracy is 0.03°C (Freitag et al., 1994). Because the MTR casing is reflective, small, and has high thermal conductivity, it is expected that there is negligible thermal warming of the sensor due to solar radiation when deployed in the euphotic zone. Thus, with the vertical and temporal resolution available here, MTR data are suitable for mixed layer studies.

3. Results

3.1. Enhanced monitoring at 0°, 110°W during the 1997–1998 El Niño

The enhanced monitoring period from August 1997 through February 1998 straddles the peak interannual SST anomalies associated with the 1997–1998 El Niño (see line indicating enhanced monitoring period in Figs. 2 and 3). For a complete discussion of the large-scale progression of the 1997–1998 El Niño, see McPhaden (1999), Johnson et al. (2000), Slingo (1998). The EMP was marked by two distinct regimes (Fig. 4). Prior to December 1997, SST at 0°, 110°W was always less than 29°C, rainfall was infrequent, and SST and sea-surface salinity (SSS) had several 20–25 day oscillations (apparently due to tropical instability waves) and minimal high frequency (diurnal) variability. Likewise, the temperature difference between 1 and 5 m was essentially zero and MLD_T showed no substantial diurnal variability. The upper ocean in fact was nearly isothermal down to ~50 m, and the depth of the 20°C isotherm (Z20) was ~125 m.

As the SST rose above 28.5°C in early December 1997, a regime shift was observed, involving an abrupt increase in rainfall and change of character of mixed-layer depth and surface temperature and salinity variability (Fig. 4). Indeed, with very warm surface temperatures, a deep thermocline, low winds, and increased convective clouds and rainfall, conditions at 0°, 110°W were more typical of the western equatorial Pacific warm pool. As in the warm pool, individual rain events showed transient SSS fresh anomalies (typically 1 PSU) lasting from a few hours to a day (Cronin and McPhaden, 1998). Consistent with freshwater stratification supporting temperature inversions (cold water above warm water), inversions often occurred during low SSS (less than ~33 PSU), and during times of heavy rain and low (less than 4 ms^{-1}) wind speeds. The vertical lines in Fig. 4 indicate periods in which subsurface temperature at any depth was more than 0.2°C warmer than SST for more than 24 h. For example, on 12 February 1998, the daily averaged 20 m temperature was more than 0.6°C greater than the SST. Likewise, on 21 February 1998, the daily averaged 10 m temperature was about 0.3°C greater than the SST. During the 3 month period from 5 December 1997 through 28 February 1998, ten inversions greater than 0.2°C and lasting longer than 24 h were observed, representing 8% of the record. Because a temperature inversion must be supported by salinity stratification to remain stable, during periods with temperature inversions, the mixed-layer depth must be shallower than MLD_T. Thus, temperature inversions can be used to infer the presence of a salinity stratified barrier layer. However, this represents only a subset of the times a barrier layer existed at this site, since periods when the barrier layer was isothermal cannot be identified without subsurface salinity data.

Although temperature inversions tended to produce a relatively deep MLD_T (and by inference a shallow MLD), on clear afternoons with weak

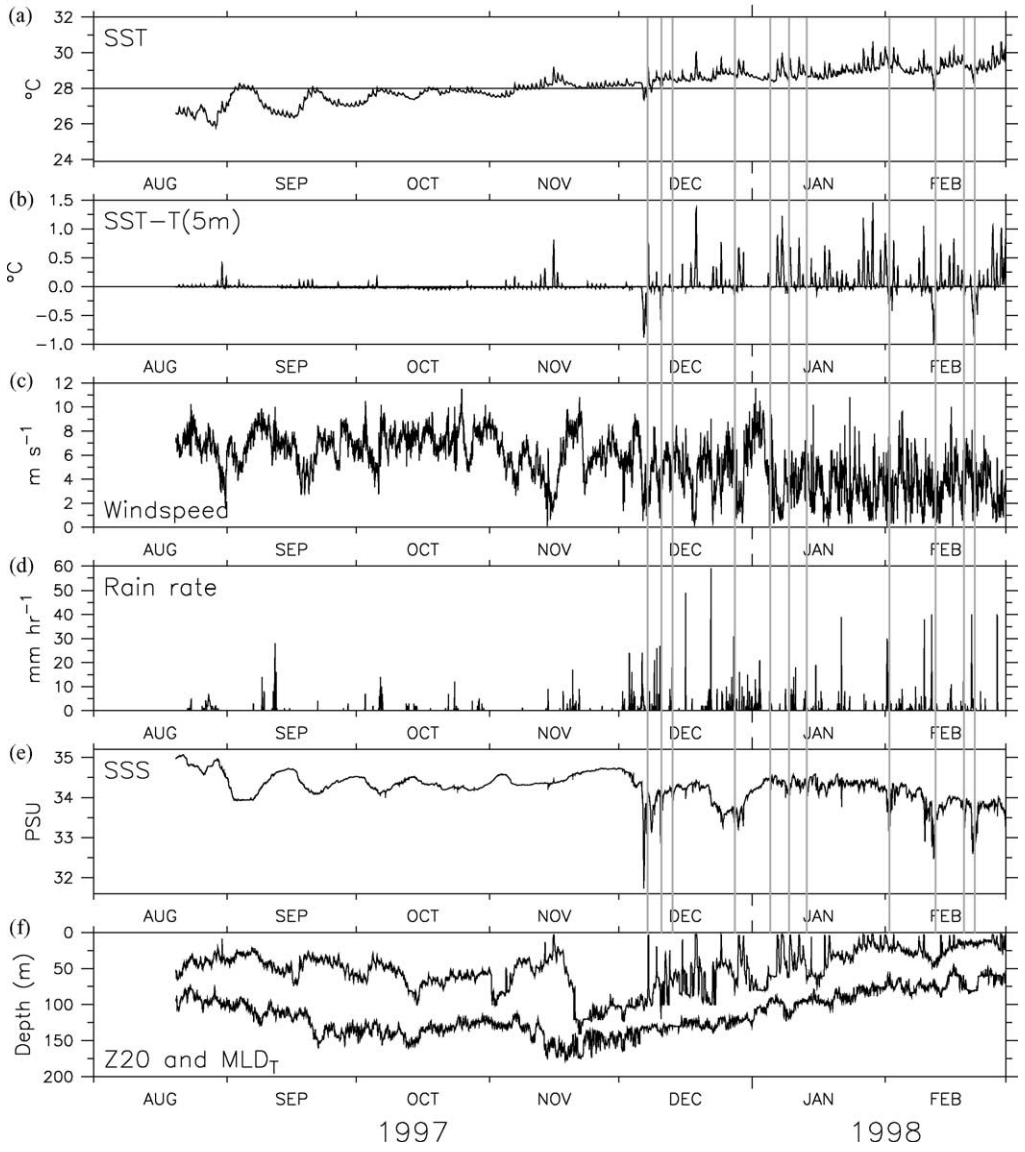

Fig. 4. Hourly time series at 0°, 110°W during the enhanced monitoring period, 20 August 1997 through 28 February 1998. (a) SST at 1 m depth (°C), (b) SST minus 5 m temperature (°C), (c) daily averaged wind speed ($m\,s^{-1}$), (d) rain rate ($mm\,h^{-1}$), (e) sea-surface salinity (practical salinity unit), and (f) Z20 and isothermal-mixed layer depth (MLD_T) (m). The vertical gray bars indicate periods when a temperature inversion greater than 0.2°C occurred for more than 24 h.

winds there was up to a 1°C temperature stratification between 1 and 5 m (Fig. 4b) so that there was essentially no mixed layer (Fig. 4f). However, even during these periods of solar-induced surface restratification, nighttime surface cooling and consequent convective mixing caused an isothermal-mixed layer to form and extend down to near the top of the thermocline. When the thermocline was deep, as it was in December 1997, daytime warming and nighttime mixing produced an MLD_T diurnal cycle ranging from near the surface to well below 50 m. However, as the

thermocline shoaled from December 1997 through February 1998, the maximum depth of the MLD_T shoaled to ~ 25 m.

Note that the coincidence of the SST and MLD_T diurnal cycles depends to a certain extent upon the choice of ΔT in the MLD_T definition (1). Although afternoon near-surface temperature stratification was at times as large as 1°C in the top 5 m, more typically, the peak-to-peak SST diurnal cycle amplitude and near-surface stratification were less than 0.5°C. Thus, MLD_T as defined by (1) did not always have a diurnal cycle associated with the SST diurnal cycle. Likewise, because the depth of nighttime mixing is limited by the thermocline's depth, the MLD_T diurnal cycle was larger when the thermocline was deeper.

In summary, during the final stages of the 1997–98 El Niño, as the "western equatorial Pacific" warm pool extended across the entire Pacific and surface waters at 0°, 110°W warmed above 28.5°C, the site experienced a regime shift with increased convective clouds and rainfall, temperature inversions, and increased SST diurnal cycle and mixed-layer depth variability. The regime shift also marked the deepest extent of the thermocline and near-isothermal layer (MLD_T). Prior to mid-November, both the thermocline and MLD_T tended to deepen (although not necessarily at the same time); after early December, both tended to shoal. Thus, in terms of the questions posed in Section 1, we find that the SST diurnal cycle does appear to have increased as SST warmed above 28.5°C, and that the nighttime mixed-layer depth tended to be deep when the thermocline was deep and shallow when the thermocline was shallow.

3.2. Annual and interannual variability at 0° 110°W

Clearly several types of mixed layer regimes occur at 0°, 110°W. However, with only a 7-month record it is not possible to determine how the December 1997 regime shift relates to the seasonal and ENSO cycles. Typically how large is the SST diurnal cycle amplitude in September versus January? Was the SST diurnal cycle amplitude during this historic El Niño warm event larger or smaller than during La Niña cool events? Are temperature inversions present in the eastern equatorial Pacific only during the final stages of El Niños? Although the mooring had best resolution during the enhanced monitoring period described above, long time series of surface and subsurface data (albeit with less vertical resolution) are available at this site. In this section we analyze the low-frequency variability of the background state, which sets the context for our analysis of the seasonal and interannual modulation of SST diurnal cycle and typically short-lived temperature inversions.

Because of extensive data gaps in the long hourly records, for this purpose, MLD_T and Z20 are computed from daily averaged temperature, rather than from hourly data. Since the Z20 calculation is linear, daily averaged Z20 is equivalent to Z20 computed from daily averaged temperature. However, this is not necessarily true for mixed-layer depth. For example, a very large daytime thermal surface stratification can appear as a weak stratification in the daily averaged temperature. Consequently, if ΔT in (1) is too small, MLD_T computed from daily averaged temperature can be shallower than the depth of nighttime mixing. We posit that ΔT should be larger than the amplitude of the SST diurnal cycle so that the daily averaged SST minus ΔT is cooler than the nighttime SST. If so, then MLD_T computed from daily averaged temperature will be a rough measure of the depth of nighttime mixing. Fig. 5 shows a comparison of MLD_T computed from hourly and daily averaged temperatures. Note that while there are occasional periods when the hourly mixed layer is deeper than MLD_T from daily averaged temperature (e.g. 2nd week of December, 2nd week of January), most of these periods appear to be associated with temperature inversions. During inversions, MLD based on density is shallower than MLD_T, and it is unlikely that mixing extends throughout MLD_T. However, in most cases, MLD_T defined by (1) and computed with daily averaged temperature appears to adequately capture the depth of nighttime mixing represented by the deep nighttime values of hourly MLD_T.

In order to analyze the seasonal and interannual variability, all variables in Fig. 6 (OLR, wind speed, SST, SST−10 m temperature, MLD_T, and

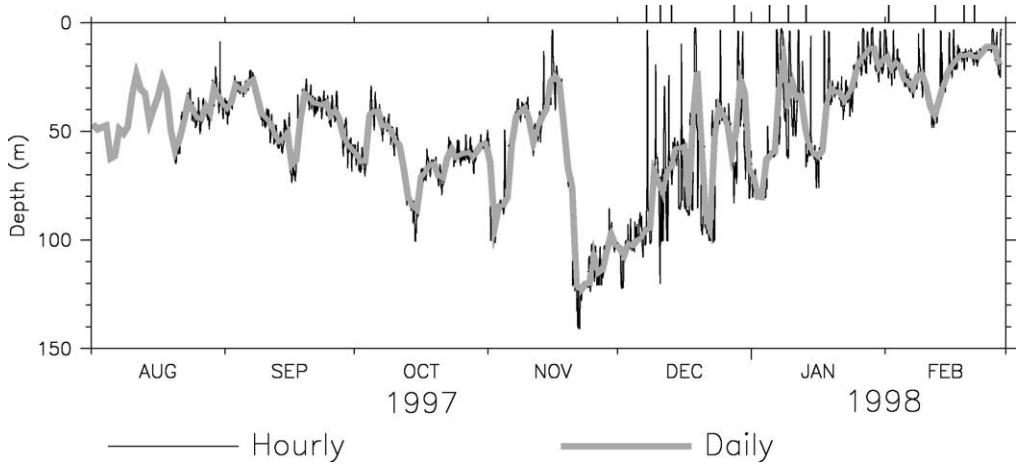

Fig. 5. MLD_T computed from hourly temperature data (thin black line) and from daily averaged temperature data (thick grey line) for the 0°, 110°W enhanced monitoring period from September 1997 through February 1998.

Z20) were monthly averaged and subsampled to once per month, then averaged to produce a seasonal climatology. The seasonal climatology was subtracted from the monthly averaged time series and smoothed with a 3-month boxcar filter to produce the interannual anomalies shown in Fig. 7. Because the vertical resolution of the subsurface temperature was typically 10–20 m, the daily MLD_T measurement error was typically 5–10 m according to (2). With an integral time scale of $\sim$10 days and assuming these to be random errors, the measurement error of the monthly averaged MLD_T is reduced by approximately $1/\sqrt{3}$ to be $\sim$3–6 m. The measurement error is further reduced by a factor of $1/\sqrt{13}$ to be 1–2 when climatologies based on 13 years of data are computed. Thus, only confidence limits for estimating climatological means for each month are shown in Fig. 6.

Although the sun crosses the equator twice per year, in March and again in September, SST has predominantly a one-cycle per year oscillation at 0°, 110°W, with a warm season from February through May, and a cold season from June through November (Fig. 6c). Consistent with the annual migration of the ITCZ, wind speed is low during the warm season when the ITCZ is closest to the equator, and high during the cold season when the ITCZ is at its northernmost latitude. Very low OLR values (signifying deep atmospheric convection) occurred at this location only during El Niños (Figs. 3 and 7). Consequently, the OLR annual cycle at 0°, 110°W was not significant at the 95% confidence level.

The thermocline depth (Z20) seasonal cycle (Fig. 6f) was also not significant at the 95% confidence level. MLD_T, however, did have a significant seasonal cycle and was shallowest during March, the warm season, when on average there was nearly a 1°C stratification in the top 10 m (Fig. 6de). As shown in the next section, the SST diurnal cycle amplitude is also larger during the warm season, suggesting that the shallow mixed layer during the warm season is due to solar-induced thermal restratification caused by seasonal weak winds and high insolation.

El Niños (1986–1987, 1991–1992, 1993, 1994–1995, and 1997–1998) and La Niñas (1988 and 1996) are clearly seen in the interannual anomaly time series shown in Fig. 7. In particular, the commonly used southern oscillation index (surface pressure difference between Darwin and Tahiti) is highly anti-correlated at zero lag with the interannual SST anomalies at 0°, 110°W. Typically, El Niño events (negative SOI) are characterized at 0°, 110°W by warm SSTs, increased convection,

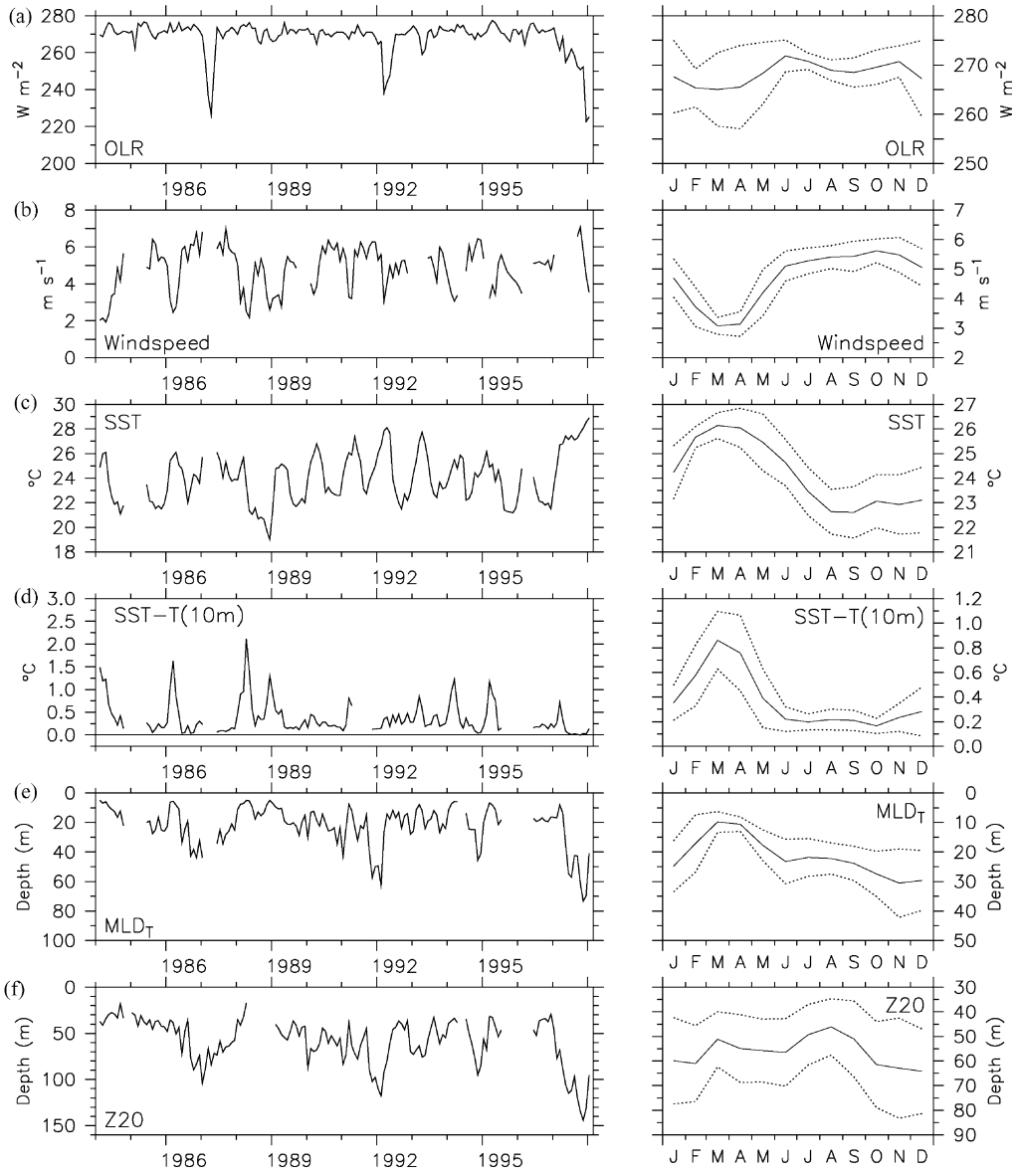

Fig. 6. Monthly averaged time series (left panels) and seasonal averages (right panels) at 0°, 110°W. (a) OLR ($W\,m^{-2}$), (b) wind speed ($m\,s^{-1}$), (c) SST (°C), (d) SST minus temperature at 10 m (°C), (e) MLD_T (m), and (f) Z20 (m). The 95% confidence level is shown for the seasonal cycles (dotted line).

slightly higher wind speeds, and deep Z20 and MLD_T. Likewise, at this location, La Niña events (positive SOI) are characterized by cooler SSTs, slightly lower wind speeds, reduced convection, and shallower thermocline and MLD_T (Fig. 7). Note that MLD_T cannot be deeper than the top of the thermocline. Therefore, when the thermocline is very shallow, as it is during La Niñas, MLD_T will correspondingly be limited in depth. For example, during the 1988 La Niña, the 20°C isotherm outcropped and there was a 2.5°C temperature difference between 1 and 10 m, indicating that

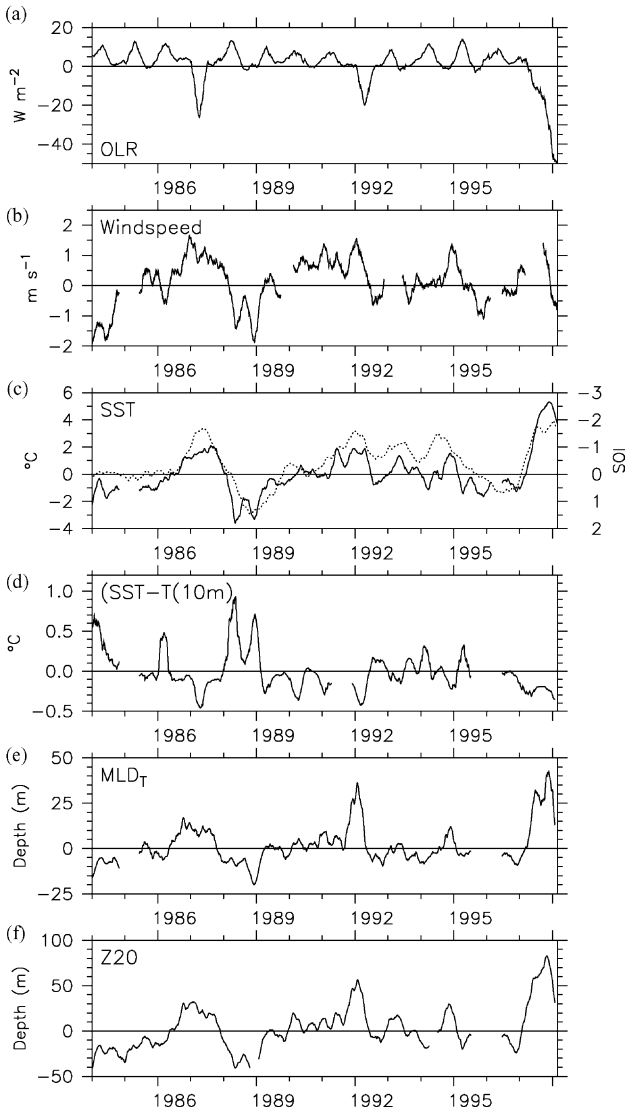

Fig. 7. Same as Fig. 6, but for interannual anomalies, smoothed with a 90-day boxcar filter. The Southern Oscillation Index (SOI) is shown as a dotted line in (c).

there was essentially no mixed layer at this time. Thus, both surface process (e.g. wind mixing and surface heating) and thermocline variability act to produce a shallow mixed layer during La Niña cold events and a deep mixed layer during El Niño warm events. Consequently, interannual Z20 and MLD_T anomalies are in phase and have a cross-correlation of 0.94.

3.3. Annual and interannual modulation of high frequency variability at 0°, 110°W

3.3.1. Temperature inversions

As illustrated during the 1997–1998 El Niño enhanced monitoring period (Fig. 4), large ($\sim$0.2°C) temperature inversions are typically short-lived. Only 11 events during the EMP had inversions

larger than 0.2°C and lasting longer than 24 h. Since a 24-h event may span parts of two different days, the inversions may appear to be weaker and longer when estimated with daily averaged temperature data centered at 12:00 GMT. However, although large inversion events may be identifiable in the daily averaged data, these short-lived events are unlikely to register in monthly averaged data. It is therefore not surprising that based on monthly averaged data, 1 m SST was always warmer than the temperature at 10 m (Fig. 6d).

To determine the prevalence of inversions, we use the long time series of daily averaged temperatures to compute temperature differences relative to 1 m SST. Fig. 8 shows for each day the maximum positive differences (i.e. inversions) that are greater than 0.03°C (the accuracy of the sensor), monthly averaged precipitation from Xie and Arkin (1995), and the SOI. Since changing vertical resolution can cause apparent changes in the magnitude of the temperature inversion, magnitudes in Fig. 8 should be viewed with caution. With these caveats, Fig. 8 shows that temperature inversions at 0°, 110°W occurred almost exclusively during the final stages of strong El Niño warm events, when winds were weak and deep atmospheric convection resulted in strong rainfall. Because the temperature inversions must be supported by a freshwater stratified barrier layer, we can conclude that barrier layers were present during these periods.

The coincidence of temperature inversions, rain events and weak winds (Figs. 4 and 8) suggests barrier layers were formed by local rain events. Near the dateline, salty warm water can be subducted under the western Pacific warm fresh water to form thick barrier layers (Lukas and Lindstrom, 1991; Vialard and Delecluse, 1998). Further study is needed to determine whether subduction also plays a role in forming barrier layers in the eastern equatorial Pacific.

3.3.2. SST diurnal cycle

The enhanced monitoring period during the 1997–1998 El Niño also showed variations in the SST diurnal cycle amplitude, with minimal diurnal cycle amplitudes before SSTs rose above 28.5°C in December 1997. In order to determine the seasonal and interannual modulation of SST diurnal cycle, we performed a complex demodulation (Bloomfield, 1976; Kessler et al., 1995) on the long time series of hourly SST. The procedure expresses SST

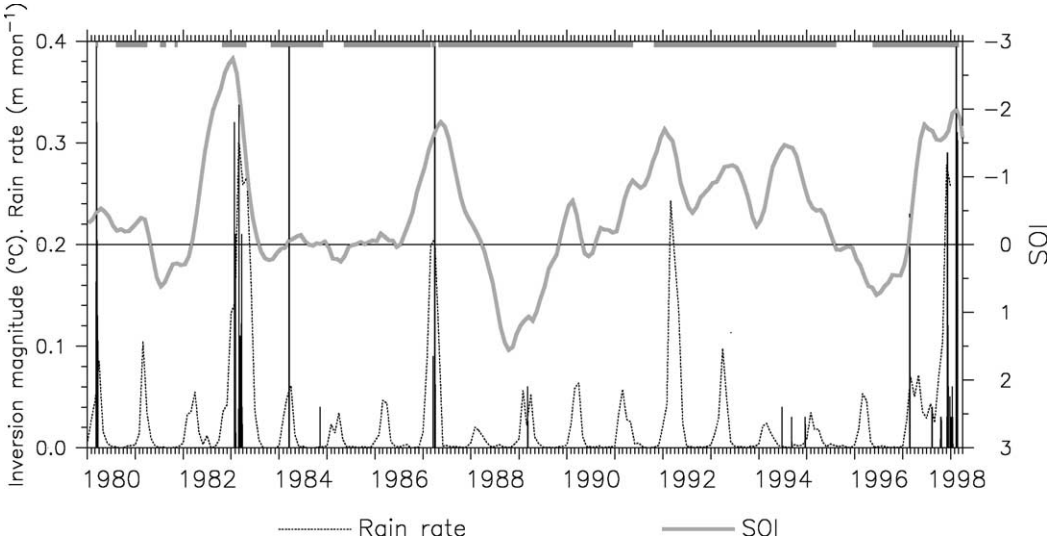

Fig. 8. Temperature inversion time series at 0°, 110°W computed from daily averaged data (solid bars), compared to the SOI (grey line) and monthly rain rates (dotted line). A negative SOI (plotted upward here) is commonly used as an indicator of an El Niño warm event. The stripe across the top of the plot shows periods when temperature inversion could be estimated. Only inversions greater than the accuracy of the sensor (0.03°C) are shown. Rain rates are from Xie and Arkin (1995).

as a diurnal cycle with slowly varying amplitude $A(t)$ and phase $\Phi(t)$ superimposed upon the rest of the variability $Z(t)$

$$SST(t) = A(t)\cos(\omega t - \Phi(t)) + Z(t),$$

where $\omega = 2\pi/\text{day}$. Peak-to-peak diurnal variations are equivalent to twice the amplitude $A(t)$. As in Figs. 6 and 7, the monthly averaged $A(t)$ time series is decomposed into annual and residual interannual components (Fig. 9). The diurnal cycle nearly always has maximum SST at 16:00 local; therefore, the phase modulation $\Phi(t)$ is not shown.

During the 8-yr record, the monthly averaged SST diurnal cycle amplitude ranged from below 0.1°C during the early part of the 1997–1998 El Niño to nearly 0.5°C during the warm seasons of 1986 and 1988 (a La Niña year) (Fig. 9). The SST diurnal cycle was modulated both by the seasonal cycle and by ENSO. During the warm season (February–April), the diurnal cycle typically had an amplitude of up to 0.4°C, but at other times of the year the amplitude was typically less than 0.2°C. The ENSO cycle caused approximately ±0.1°C variations in the SST diurnal amplitude,

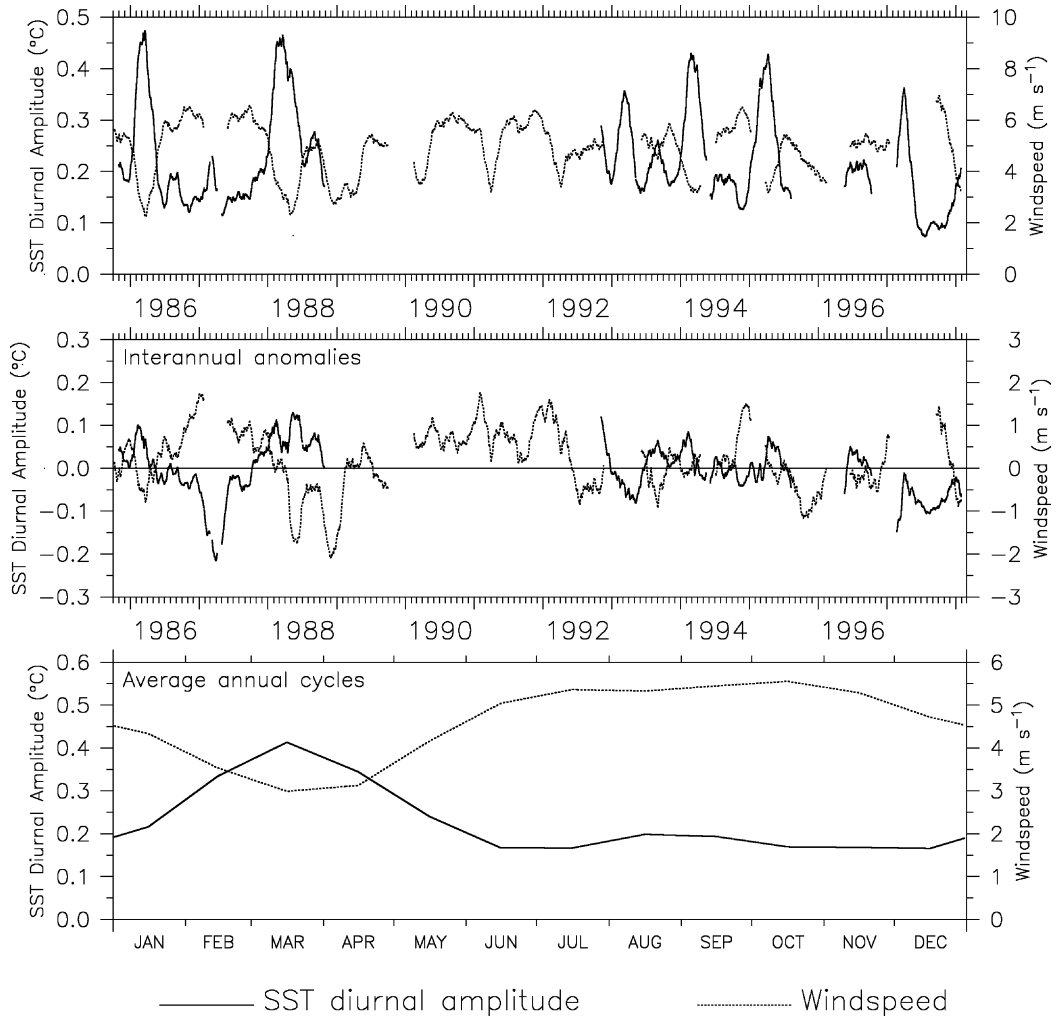

Fig. 9. SST diurnal cycle amplitude (solid line; °C) and wind speed (dotted line; m s^{-1}). Top panel: amplitude time series. Middle panel: interannual anomalies. Bottom panel: seasonal cycles.

with higher amplitudes during La Niñas and lower amplitudes during El Niños. On both the seasonal and interannual time scales, the SST diurnal cycle amplitude varied in relation to local winds and deep atmospheric convection, with higher amplitudes during periods of weak winds and clear skies, and lower amplitudes during periods of strong winds and deep atmospheric convection (Figs. 6 and 9). Although the SST diurnal cycle increased following the December 1997 regime shift (Fig. 4), it was still weaker than typically found during warm seasons because of the reduced insolation associated with this historic El Niño.

4. Discussion and summary

In answer to the first question stated in Section 1, "is the SST diurnal cycle amplitude largest during warm phases of the seasonal and ENSO cycles?", we find that on seasonal time scales, SST diurnal cycle amplitude is largest during the warm season; but on interannual timescales, the SST diurnal cycle is largest during the cold phase of ENSO. These results highlight the different physics at play on these two timescales. Surface heating and local wind-forced upwelling and mixing are dominant processes controlling seasonal SST variability, but are secondary processes on ENSO time scales.

Although the sun crosses the equator twice per year, in March and again in September, SST is warmest during February through April and coolest during August through October. Heat balance analyses of this region (Enfield, 1986; Hayes et al., 1991; Kessler et al., 1998; Swenson and Hansen, 1999; Wang and McPhaden, 1999) attribute the seasonal variations to a variety of processes, including the equinoctial increase in solar radiation, changes in upwelling and turbulent mixing associated with the local trade wind forcing, meridional heat fluxes associated with tropical instability waves, and the reduction in solar radiation due to the extensive stratocumulus decks that cover the eastern Pacific during August to November. Of these seasonal heating and cooling processes, only the tropical instability waves have no corresponding effect on the SST diurnal cycle modulation. Local wind forcing and surface heating processes that produce seasonal warming and cooling also increase and decrease the SST diurnal cycle amplitude. For example, weaker wind speeds and stronger solar radiation in March contribute to both seasonal warming and an increased SST diurnal cycle. For this reason, the seasonal modulation of the SST diurnal cycle is in phase with the SST seasonal cycle.

In contrast, interannual variations in east Pacific SST are controlled primarily by large-scale three-dimensional processes. Shifts in the western and central Pacific trade winds generate Kelvin waves, which result in a basin-wide adjustment of the thermocline depth. During La Niñas, maximum trade winds and deep atmospheric convection shift westward, resulting in clear skies and relatively weak winds and consequently anomalously high diurnal cycle amplitude (1°C) in the eastern equatorial Pacific. During El Niños, the reverse occurs (Rasmusson and Carpenter, 1982; Harrison and Larkin, 1998). In particular, during the early stage of the 1997–1998 El Niño warm event, maximum trade winds shifted eastward so that wind speeds were anomalously high at 0°, 110°W through October 1997. Then as the waters warmed above ~28.5°C in December 1997, deep convective clouds shifted eastward and the winds weakened (Figs. 2 and 3). Thus, first higher winds and then to a lesser extent deep tropical convection at 0°, 110°W caused the SST diurnal cycle amplitude to be anomalously low (−1°C to −0.5°C) during the 1997–98 El Niño warm event. Consistent with empirical interannual heat budgets (Wang and McPhaden, 2000), on ENSO timescales, local surface heating acts as a damping term, tending to warm the SSTs during La Niña cold events and cool the surface during El Niño warm events.

The second question posed in Section 1 was whether the thermocline displacements could be used as a proxy for mixed-layer depth variations. The isothermal-mixed layer depth (MLD_T) is always shallower than the thermocline depth as represented by the depth of the 20°C isotherm (Z20); mean depths of these two surfaces are 22 and 58 m (Table 1). Likewise, interannual MLD_T anomalies are smaller than Z20 anomalies. As shown in Table 1, interannual anomalies have

Table 1
Standard deviations and means of variables shown in Figs. 6 and 7 (outgoing longwave radiation (OLR), wind speed, sea-surface temperature at 1 m (SST), temperature difference between 1 and 10 m, isothermal-mixed layer depth (MLD_T) defined by (1), and depth of the 20°C isotherm (Z20)). Standard deviations of the annual cycle amplitude, interannual anomalies, and monthly averaged time series are listed. Annual cycles that are significantly different than zero at the 95% confidence limit are indicated in bold

	Standard deviations			
	Annual cycle	Interannual anomalies	Monthly averages	Means
OLR (Wm^{-2})	2	9	9	269
Wind speed (ms^{-1})	**0.88**	0.86	1.21	4.80
SST (°C)	**1.31**	1.61	2.02	24.03
SST - T(10 m) (°C)	**0.22**	0.28	0.36	0.37
MLD_T (m)	**6**	12	14	22
Z20 (m)	6	24	25	58

standard deviations of 12 m for MLD_T and 24 m for Z20. However, with these caveats, on interannual time scales, Z20 can be used as a proxy for MLD_T variability since these two surfaces are well correlated (0.94), both being deep during El Niño warm events and anomalously shallow during La Niña events. However, on seasonal timescales, MLD_T and thermocline depth tend to be unrelated (Fig. 6). The isothermal-mixed layer depth is shallowest during the warm season, March, and deepest in November, with a standard deviation of 6 m (Table 1). In contrast, the thermocline depth seasonal cycle is not significant at the 95% confidence level. Thus, on seasonal timescales, thermocline depth cannot be used as a proxy for mixed-layer depth.

In general, mixed-layer depth should be defined in terms of density rather than temperature. In particular, if the near surface is stratified in salinity but not in temperature, the isothermal layer between the shallow halocline and the top of the thermocline can act as a barrier to turbulent entrainment of cool thermocline water into the surface mixed layer (Lukas and Lindstrom, 1991). Cooling processes at the surface and solar radiation penetrating into the salinity stratified 'barrier layer' can cause temperature inversions to develop without causing the density profile to become convectively unstable (Anderson et al., 1996). In this case, turbulent entrainment of warm barrier layer water produces surface warming. In the eastern Pacific, salinity effects are usually ignored since the thermocline is shallow and evaporation dominates over precipitation. Furthermore, using Levitus (1982) climatological data, Sprintall and Tomczak (1992) showed that there was essentially no mean barrier layer in the eastern equatorial Pacific. However, based on CTD data collected from 1976 to 1994, Ando and McPhaden (1997) showed that the composite El Niño had a 10–20 m thick barrier layer across the entire equatorial Pacific.

Although no subsurface salinity data is available at the 0°, 110°W TAO mooring, temperature inversions, implying a shallow halocline and the presence of a barrier layer, were observed during periods of high rainfall and weak winds. Following the regime shift in early December 1997, temperature inversions greater than 0.2°C and lasting longer than a day made up 8% of the record. Over the full 18 year time series of daily averaged subsurface temperature, inversions were observed almost exclusively during El Niño warm events, and primarily during the two "El Niños of the century" (1982–1983 and 1997–1998). During these warm events, the inversions were frequent and were often greater than 0.1°C when averaged over a day. Since it is possible to have a barrier layer without having a temperature inversion, barrier layers must have occurred even more frequently than this. Since barrier layers shield the surface from turbulent mixing of cold thermocline water, it is likely that the barrier layer supporting these temperature inversions helped maintain warm SSTs even as the thermocline shoaled during the termination of the El Niño.

Although the ocean is forced by the atmosphere, the atmosphere also responds to ocean surface conditions. In particular, based on the coupled ocean atmosphere response experiment (COARE) bulk flux algorithm (Fairall et al., 1996a, b; Cronin and McPhaden, 1997), a $\pm 0.5^{\circ}$C SST variation from mean conditions at 0°, 110°W can cause a $\pm 12\,\mathrm{W m^{-2}}$ latent heat flux variation and a $\pm 4\,\mathrm{W m^{-2}}$ sensible heat flux variation. Thus, the SST diurnal cycle modulation may also be associated with a modulation of the latent and sensible heat fluxes.

Similarly, SST variations also affect carbon dioxide (CO_2) flux between the ocean and atmosphere. For most of the world's oceans, the thermodynamic effect of SST variations on the partial pressure of carbon dioxide is approximately 4.23% per 1°C (Takahashi et al., 1993). Often, "surface" hydrographic bottle measurements are at 10 m depth and underway ship intake surface measurements are at 5–8 m depth. As discussed by McNeil and Merlivat (1996), daytime temperature stratification above 10 m depth can cause a 2% increase in the daily sea-to-air CO_2 flux in the eastern equatorial Pacific and a 20% increase in the western equatorial Pacific. In addition, trapping within the shallow warm layer may also affect the surface dissolved gas concentration and thus the air–sea flux. Our results suggest that this diurnal pumping will have seasonal and interannual modulations. Surface conditions should be measured well above 10 m during the warm season (February–April) and during La Niña cold events (Figs. 6 and 7).

At the equator, zonal trade winds can cause substantial upwelling, mixing, and surface cooling. The resulting SST gradients in turn affect the winds and cloud structure, causing the ocean-atmosphere system to be highly coupled. Understanding the processes by which the mixed layer properties vary is essential for quantitative diagnostics of the coupled ocean and atmosphere system and its effect on the biogeochemical ecosystem.

Acknowledgements

The authors wish to thank Chris Sabine for helpful discussions, and Michael McPhaden, Paul Freitag, and the TAO Project Office for their effort in providing this data set. Paul Freitag played a critical role in collecting the extra thermistor data on the August 1997 deployment. Funding for the raingauge and salinity sensor was provided in part by the NASA TRMM program. Funding for this analysis was provided by NOAA's Office of Global Programs. This is NOAA Pacific Marine Environmental Laboratory contribution No. 2246.

References

Anderson, S.P., Weller, R.A., Lukas, R., 1996. Surface buoyancy forcing and the mixed layer of the western equatorial Pacific warm pool: observations and 1-D model results. Journal of Climate 9, 3056–3085.

Ando, K., McPhaden, M.J., 1997. Variability of surface layer hydrography in the tropical Pacific ocean. Journal of Geophysical Research 102, 23063–23078.

Bloomfield, P., 1976. Fourier Decomposition of Time Series: An Introduction. Wiley, New York, 258pp.

Bond, N.A., McPhaden, M.J., 1995. An indirect estimate of the diurnal cycle in upper ocean turbulent heat fluxes at the equator, 140°W. Journal of Geophysical Research 100, 18369–18378.

Cronin, M.F., McPhaden, M.J., 1997. The upper ocean heat balance in the western equatorial Pacific warm pool during September–December, 1992. Journal of Geophysical Research 102, 8533–8553.

Cronin, M.F., McPhaden, M.J., 1998. Upper ocean salinity balance in the western equatorial Pacific. Journal of Geophysical Research 103, 27567–27587.

Deser, C., Wallace, J.M., 1987. El Niño events and their relation to the southern oscillation: 1925–1986. Journal of Geophysical Research 92, 14189–14196.

Enfield, D.B., 1986. Zonal and seasonal variations in the near-surface heat balance of the equatorial ocean. Journal of Physical Oceanography 16, 1038–1054.

Fairall, C., Bradley, E.F., Rogers, D.P., Edson, J.B., Young, G.S., 1996a. Bulk parameterization of air-sea fluxes for tropical ocean-global atmosphere coupled-ocean atmosphere response experiment algorithm. Journal of Geophysical Research 101, 3747–3764.

Fairall, C., Bradley, E.F., Godfrey, J.S., Wick, G.A., Edson, J.B., Young, G.S., 1996b. Cool skin and warm layer effects on sea surface temperature. Journal of Geophysical Research 101, 1295–1308.

Freitag, H.P., Feng, Y., Mangum, L.J., McPhaden, M.J., Neaner, J., Stratton, L.D., 1994. Calibration procedures and instrumental accuracy estimates of TAO temperature, relative humidity and radiation measurements. NOAA Technical Memo. ERL PMEL-104, 32 pp. Pacific Marine Environmental Laboratory, NOAA, Seattle, WA.

Halpern, D., 1987. Observations of annual and El Niño thermal and flow variations at 0°, 110°W and 0°, 95°W during 1980–1985. Journal of Geophysical Research 92, 8197–8212.

Halpern, D., Knox, R.A., Luther, D.S., 1988. Observations of 20-day period meridional current oscillations in the upper ocean along the Pacific equator. Journal of Physical Oceanography 18, 1514–1534.

Harrison, D.E., Larkin, N.K., 1998. El Niño-Southern Oscillation sea surface temperature and wind anomalies, 1946–1993. Reviews of Geophysics 36, 353–399.

Hayes, S.P., Chang, P., McPhaden, M.J., 1991. Variability of the sea surface temperature in the eastern equatorial Pacific during 1986–1988. Journal of Geophysical Research 96, 10553–10566.

Johnson, G.C., McPhaden, M.J., Rowe, G.D., McTaggart, K.E., 2000. Upper equatorial Pacific ocean current and salinity variability during the 1996–1998 El Niño–La Niña cycle. Journal of Geophysical Research 105, 1037–1053.

Kessler, W.S., McPhaden, M.J., Weickman, K.M., 1995. Forcing of intraseasonal Kelvin waves in the equatorial pacific. Journal of Geophysical Research 100, 10613–10631.

Kessler, W.S., Spillane, M.D., McPhaden, M.J., Harrison, D.E., 1996. Scales of variability in the equatorial Pacific inferred from the tropical atmosphere-ocean (TAO) buoy array. Journal of Climate 9, 2999–3024.

Kessler, W.S., Rothstein, L.M., Chen, D., 1998. The annual cycle of SST in the eastern tropical pacific, diagnosed in an ocean GCM. Journal of Climate 11, 777–799.

Levitus, S., 1982. Climatological atlas of the world ocean. NOAA Prof. Pap. 13, 173 pp., US Government Printing Office, Washington, D.C.

Lewis, E.L., Fofonoff, N.P., 1979. A practical salinity scale. Journal of Physical Oceanography 9, 446–446.

Lukas, R., Lindstrom, E., 1991. The mixed layer of the western equatorial Pacific Ocean. Journal of Geophysical Research Supplement 96, 3343–3357.

McNeil, C.L., Merlivat, L., 1996. The warm oceanic surface layer: implications for CO_2 fluxes and surface gas measurements. Geophysical Research Letters 23, 3575–3578.

McPhaden, M.J., 1999. Genesis and evolution of the 1997–98 El Niño. Science 283, 950–954.

McPhaden, M.J., et al., 1998. The tropical ocean global atmosphere (TOGA) observing system: a decade of progress. Journal of Geophysical Research 103, 14169–14240.

Moum, J.N., Caldwell, D.R., Paulson, C.A., 1989. Mixing in the equatorial surface layer and thermocline. Journal of Geophysical Research 94, 2005–2021.

Peters, H., Gregg, M.C., Sanford, T.B., 1994. The diurnal cycle of the upper equatorial ocean: Turbulence, fine-scale shear, and mean shear. Journal of Geophysical Research 99, 7707–7723.

Qiao, L., Weisberg, R.H., 1995. Tropical instability wave kinematics: observations from the tropical instability wave experiment. Journal of Geophysical Research 100, 8677–8693.

Qiao, L., Weisberg, R.H., 1998. Tropical instability wave energetics: observations from the tropical instability wave experiment. Journal of Physical Oceanography 28, 345–360.

Rasmusson, E.M., Carpenter, T.H., 1982. Variations in tropical sea surface temperature and surface wind fields associated with the southern oscillation/El Niño. Monthly Weather Review 110, 354–384.

Slingo, J., 1998. The 1997/98 El Niño. Weather 53, 274–281.

Sprintall, J., Tomczak, M., 1992. Evidence of the barrier layer in the surface layer of the tropics. Journal of Geophysical Research 97, 7305–7316.

Swenson, M.S., Hansen, D.V., 1999. Tropical Pacific ocean mixed layer heat budget: the Pacific cold tongue. Journal of Physical Oceanography 29, 83–91.

Takahashi, T., Olafsson, J., Goddard, J.G., Chipman, D.W., Sutherland, S.C., 1993. Seasonal variations of CO_2 and nutrients in the high-latitude surface oceans: a comparative study. Global Biogeochemical Cycles 7, 843–878.

Vialard, J., Delecluse, P., 1998. An OGCM study for the TOGA decade. Part II: barrier-layer formation and variability. Journal of Physical Oceanography 28, 1089–1106.

Wang, W., McPhaden, M.J., 1999. The surface layer heat balance in the equatorial Pacific ocean, Part I: mean seasonal cycle. Journal of Physical Oceanography 29, 1812–1831.

Wang, W., McPhaden, M.J., 2000. The surface-layer heat balance in the equatorial Pacific ocean, Part II: interannual variation. Journal of Physical Oceanography 30, 2989–3008.

Xie, S.-P., 1995. Interaction between the annual and interannual variations in the equatorial Pacific. Journal of Physical Oceanography 25, 1930–1941.

Xie, P., Arkin, P.A., 1995. An intercomparison of gauge observations and satellite estimates of monthly precipitation. Journal of Applied Meteorology 34, 1143–1160.